A New Linear Distorted Wave Inversion Method for Microwave Imaging via Virtual Experiments

A New Linear Distorted Wave Inversion Method for Microwave Imaging via Virtual Experiments

Loreto Di Donato, *Member, IEEE*, Roberta Palmeri, *Student Member, IEEE*, Gino Sorbello, Tommaso Isernia, *Senior Member, IEEE* and Lorenzo Crocco, *Senior Member, IEEE*

***Abstract*—A novel microwave imaging approach to reconstruct the dielectric properties of target hosted in partially-known, non canonical, scenarios is proposed and assessed. The method takes joint advantage of the recently introduced "virtual experiments" paradigm and exploits a new linear approximation developed within such a framework. Such an approximation implicitly depends on the unknown targets and therefore has a broader applicability as compared to the traditional distorted Born approximation. Being non-iterative, the resulting distorted-wave inversion method is capable of quasi-real time imaging results and successfully images non-weak perturbations. The performances of the novel imaging method have been assessed with simulated data and validated experimentally against some of Fresnel datasets.**

***Index Terms*—Microwave Imaging, Distorted Born Approximation, Virtual Scattering Experiments, Linear Sampling Method.**

I. Introduction

MICROWAVE imaging techniques [1] aim at the characterization of morphological and electromagnetic properties of unknown scenarios that are not directly accessible. As such, they are relevant to a number of applications ranging from non-invasive diagnostics, to biomedical monitoring and subsurface prospections, only to mention some examples.

Such a goal is pursued by means of the solution of a non-linear and ill-posed inverse scattering problem [2], so that the development and improvement of effective solution techniques is a crucial issue to enable the above mentioned applications and possibly open the way to new ones. On the other hand, such a task is nontrivial, as it requires to develop suitable techniques [3] to defeat the problem's ill-posedness, as well as difficulties arising from its non-linearity. In this respect, the problem is typically cast into an iterative optimization of a cost functional whose global minimum defines the sought solution. Unfortunately, owing to the large number of unknown parameters involved in such an optimization, *global* search algorithms are not viable, but for special cases, and the optimization is carried out within *local* schemes. As known, the outcome of these latter depends on the starting point, so that the procedure may get trapped into local minima [4] and hence return an estimate which is totally different from the ground truth, the so-called *false* solution.

For such a reason, there has been persistent attention to the development of methods based on the linearization of the scattering problem. In particular, this is practically relevant to some imaging applications, wherein the target of the imaging task can be conveniently modeled as the perturbation of a known, or partially known, non-homogeneous scenario. As a matter of fact, as long as the perturbation is not too large, the problem can be linearized, thus avoiding the possible occurrence of false solutions. This is for instance the case of non-destructive testing (NDT) [5], medical imaging for follow-up purposes [6], and in general of all those situations wherein differential monitoring of changes is of interest (including through-the-wall imaging applications [7]).

While this class of methods has been originally inspired by the possibility of using, if available, a closed form solution of the fields in the reference scenario, their interest is nowadays motivated by the possibility of modeling complex, non-canonical scenarios via accurate and efficient numerical tools, so to conveniently tackle real-world scenarios.

The basic and cornerstone contribution in such a framework is the well known distorted wave Born approximation (DWBA) [8]. In this approach, the problem is formulated as the search of the difference in the permittivity distribution with respect to a nominal ground-truth by processing the anomalous field. In doing so, the DWBA approximates the internal field with the background one, thus neglecting the effect of the "perturbation" on the field. This is, from a conceptual point of view, the same limitation underlying the first order Born approximation (BA), where the effect of the scatterer on the incident field in the investigation domain is completely neglected. As a result, this leads to a linearization of the problem that is seldom fulfilled in practical instances.

A possible way to overcome this limitation is recurring to an iterative procedure (i.e., the distorted Born iterative method (DBIM) [9]–[13]). However, besides requiring the solution of several forward problems, the final outcome of such an approach depends on the starting point as well as on the validity of intermediate linearizations. Other possibilities to enlarge the range of applicability of linear inversion methods are given by the Rytov approximation [14], [15] as well as by the extended Born approximation (EBA) [16], [17] and the diagonalized contrast source (DCSI) [18] inversion approaches proposed by Habashy and co-workers. However, the Rytov

This is the post peer-reviewed version of the following article: L. Di Donato, R. Palmeri, G. Sorbello, T. Isernia and L. Crocco, "A New Linear Distorted-Wave Inversion Method for Microwave Imaging via Virtual Experiments," in IEEE Transactions on Microwave Theory and Techniques, vol. 64, no. 8, pp. 2478-2488, 2016. Article has been published in final form at: https://ieeexplore.ieee.org/document/7523398. DOI: 10.1109/TMTT.2016.2584604.

approximation only can hold true in case of smoothly varying targets [19] so that it can seldom be used.

Whereas the approaches in [16], [17] are based on peculiar assumptions which are not always satisfied (see the following), it makes sense to look for alternative more general approaches.

To address this goal, we exploit the concept of "virtual scattering experiments", which has been recently proposed to solve 2D inverse scattering problems in free space [20]–[22].

Such a concept is based on the simple, but powerful, observation that proper, data-driven, superpositions of the available scattering experiments can be interpreted as *virtual* experiments, wherein one can enforce and take advantage of some peculiar property or behavior on the (virtual) internal field and contrast source. A number of interesting results have been proposed starting from this concept, namely: a new scattering approximation [23], [24] that largely outperforms the traditional Born approximation [25] and can be the "engine" of a new inversion method based on successive linearizations [26]; a new regularization strategy for non-linear iterative inversion schemes [27] and a completely new way to solve the non-linear inverse scattering problem through an algebraic method [28]. Last, but not least, the virtual experiments provide an effective framework for the exploitation of compressive sensing techniques in inverse scattering [29].

As all the above results have been derived in the case of free space or homogeneous media, in this paper we generalize the linear inversion method introduced in [23] to the case of a partially known, nonhomogeneous scenarios and exploit it to appraise the properties of non-weak anomalies. To this end, the key step is to extend the concept of virtual experiments from the so far considered canonical case to the case of a non-homogeneous scenarios. In practice, this is done by exploiting the "distorted" version of the linear sampling method (LSM) proposed in [31]. Notably, such an imaging approach has been developed for retrieving the shape of unknown targets hosted in partially known, non-homogeneous scenarios, whereas we use here as a tool to design the virtual experiments. The distorted LSM is based on the solution of a linear problem and the virtual experiments allow to introduce an approximated (but target-aware) linear relationship between the data and the unknown. Hence, the overall method is based on the noniterative solution of two linear problems, and it is therefore extremely effective from a computational point of view.

The paper is structured as follows. In Section II, the imaging problem is formulated and the traditional distorted-wave Born approximation is recalled. In Sections III, the virtual experiments driven approximation is introduced, together with the strategy pursued to design the relevant virtual experiments. In Section IV, the new distorted-wave inversion method is presented, by describing its implementation steps, while Section V is concerned with the method's validation with simulated and experimental data. Conclusions follow. Throughout the paper, we consider the 2D scalar problem, non magnetic objects and the time factor $exp\{j\omega t\}$ is assumed and dropped.

II. The imaging problem and the standard distorted-wave approximation

Let Σ be the region of interest (ROI) of the imaging problem, given by the cross section of an infinite cylinder with non homogeneous relative complex permittivity distribution $\tilde{\varepsilon}(\underline{r})$. Given the invariance of the problem along the z-axis, we consider the 2D scalar formulation of the electromagnetic scattering problem and assume the TM polarization for the electric field. We assume that the relative permittivity distribution within the ROI is partially known so that the complex permittivity in the whole space can be expressed as

$$\tilde{\varepsilon}(\underline{r}) = \tilde{\varepsilon}_b(\underline{r}) + \delta\tilde{\varepsilon}(\underline{r}), \tag{1}$$

with:

$$\tilde{\varepsilon}_b(\underline{r}) = \begin{cases} \tilde{\varepsilon}_1(\underline{r}) & \underline{r} \in \Sigma \\ \tilde{\varepsilon}_{host} & \underline{r} \notin \Sigma \end{cases} \tag{2}$$

wherein $\underline{r} = (x, y)$, $\tilde{\varepsilon}_{host}$ is the complex permittivity of the homogeneous medium which surrounds Σ and $\tilde{\varepsilon}_1$ denotes the "nominal" relative permittivity distribution in Σ, i.e., when no perturbation is present. Note that, for the sake of simplicity, we are assuming that the medium outside the ROI is homogeneous. However, the following discussion holds true also for the general inhomogeneous case. Saying it in other words, (2) expresses the complex permittivity of the scenario at hand as a "perturbation" with respect to a nominal background permittivity distribution.

By considering N transmitting and M receiving probes positioned on a curve Γ external to the ROI, the anomalous field ΔE_s^ν produced by the perturbation $\delta\tilde{\varepsilon}$ for the generic ν-th transmitting probe is expressed by the integral equation (the *data* equation)

$$\begin{aligned} \Delta E_s^\nu(\underline{r}) = \int_\Sigma g_b(\underline{r}', \underline{r}) E_t^\nu(\underline{r}') \delta\tilde{\varepsilon}(\underline{r}') d\underline{r}' = \\ = \mathcal{A}_e[\delta\tilde{\varepsilon} E_t^\nu], \quad \underline{r} \in \Gamma \end{aligned} \tag{3}$$

where E_t^ν denotes the total field, which in turn is given by the *internal* integral equation:

$$\begin{aligned} E_t^\nu(\underline{r}) = E_b^\nu(\underline{r}) + \int_\Sigma g_b(\underline{r}', \underline{r}) E_t^\nu(\underline{r}') \delta\tilde{\varepsilon}(\underline{r}') d\underline{r}' = \\ = E_b^\nu + \mathcal{A}_i[\delta\tilde{\varepsilon} E_t^\nu], \quad \underline{r} \in \Sigma \end{aligned} \tag{4}$$

$E_b^\nu(\underline{r})$ being the background field arising in the reference scenario when the ν-th probe is active.

In (3) and (4) g_b denotes the Green's function for the assumed background scenario, $\left[\nabla^2 + k_b^2(\underline{r})\right] g_b(\underline{r}', \underline{r}) = \delta(\underline{r}' - \underline{r})$, with k_b being the reference scenario wavenumber. Typically, this function is not known in a closed form and it is computed numerically. $\mathcal{A}_e[\cdot] : L^2(\Sigma) \rightarrow L^2(\Gamma)$ is the short notation of the radiation operator that relates the contrast source $\delta\tilde{\varepsilon} E_t$ to the anomalous field on Γ, while the operator $\mathcal{A}_i[\cdot] : L^2(\Sigma) \rightarrow L^2(\Sigma)$, relates the contrast source to the field it radiates in Σ.

It is worth noting that the knowledge of the reference scenario is also exploited to appraise the scattered field perturbation ΔE_s starting from the quantity actually measured by the receiving probes, say M_t, which is affected by both

the perturbation and the reference scenario. Accordingly, it is possible to extract the required field from this latter as:

$$\Delta E_s^\nu(\underline{r}) = M_t^\nu(\underline{r}) - M_b^\nu(\underline{r}) \tag{5}$$

where,

$$M_b^\nu(\underline{r}) = E_{inc}^\nu(\underline{r}) + \int_\Sigma g_h(\underline{r}', \underline{r}) E_b^\nu(\underline{r}')[\tilde{\varepsilon}_1(\underline{r}') - \tilde{\varepsilon}_{host}] d\underline{r}' \tag{6}$$

with $E_{inc}^\nu(\underline{r})$ the field radiated by the transmitting antennas in the host medium and g_h denoting the Green's function of the same homogeneous medium. Note that, depending on the imaging problem at hand, $M_b^\nu(\underline{r})$ can be actually measured (if the "perturbation" arises in the nominal background) or estimated by properly simulating the reference scenario.

The traditional distorted wave Born approximation descends from the above equations by assuming that the variation $\delta\tilde{\varepsilon}$ is such to induce only a negligible perturbation of the background field E_b. Accordingly, the data equation (3) is approximated as:

$$\Delta E_s^\nu(\underline{r}) = \mathcal{A}_e[\delta\tilde{\varepsilon} E_b^\nu], \qquad \underline{r} \in \Gamma \tag{7}$$

and the imaging task is reduced to the solution of a linear ill-posed inverse problem.

Obviously, when the reference scenario corresponds to a homogeneous unbounded medium, this approximation exactly coincides with the classic Born approximation, so that the DWBA will be subject to the same restrictions (in terms of applicability). In particular, the approximation is expected to be successful as long as the perturbation is small enough with respect to the background wavelength and its dielectric properties are close to those of the ROI Σ [14].

III. Virtual experiments driven distorted-wave approximation

To overcome the above recalled limitations, we generalize a recently introduced approximation [23], which has the peculiarity of depending on the unknown target (in an implicit fashion), and allows to reliably linearize inverse scattering problems in a much broader range of cases as compared to BA [23], [25].

Such an approximation relies on the *virtual experiments* concept, according to which it is possible to exploit a weighted superposition of the incident fields to enforce some desired behavior of total fields (and contrast sources), to make the imaging task simpler and/or more reliable [23], [27], [30], [31]. Notably, this is done by post-processing available data and fields, without additional experiments. In fact, the only additional task is the determination of the superposition coefficients.

A. Designing virtual experiments in partially known scenarios

To apply the above concepts to the problem of imaging a perturbation in a partially know scenario, the first issue to face is how to design the virtual experiments. In practice, this is done by playing with the original incident fields and the corresponding scattered fields. However, as the incident fields do not depend on the scatterers, such a design equation has to be based on the scattered fields data.

In the free space case so far considered for the virtual experiments framework, such a design has been carried out, among other possible choices, by exploiting the LSM equation as a way to condition the scatterers behavior with respect to some points of the ROI [23]. As a matter of fact, the LSM is known to be applicable to a broad range of problems (e.g. non-weak scatterers, multiple targets and so on) and also provides an estimate of the shape of the targets (or their convex envelope), which is obviously useful for imaging purposes [32], [33]. However, the basic formulation of the LSM is valid for canonical formulation, and therefore not directly applicable in our case [32]. The problem of retrieving the shape of targets hosted in a partially known non canonical scenario has been faced in [34], wherein the necessary steps to generalize the LSM to this case have been defined and tested. The resulting distorted LSM equation is what we will use herein to design the virtual experiments. With respect to the notation we are adopting, such an equation reads:

$$[\boldsymbol{\Delta}\mathbf{E}_s][\boldsymbol{\xi}] = [\mathbf{g}_b] \tag{8}$$

wherein,

- $\boldsymbol{\Delta}\mathbf{E}_s$ is a $N \times M$ matrix whose entries are the samples of the anomalous field collected for all the N incident fields at the M receivers locations, and are computed using (5);
- $\mathbf{g}_b$ is $M \times S$ vector that contains the samples of the Green's function of the assumed background scenario at the M receivers for an arbitrary grid of S points in Σ;
- $\boldsymbol{\xi}$ is the $N \times S$ unknown vector, whose columns provide, for each point of the sampling grid, the coefficients of the corresponding virtual experiment.

The virtual experiments designed through (8) make use of the available knowledge on the scenario at hand, since they force the unknown perturbation to scatter a wave that matches on Γ the background Green's function for the considered sampling point in the ROI. While the impact of such a choice will be discussed later, let us note here that (8) corresponds to the linear sampling method (LSM) equation as developed in [34] for the case of non homogeneous backgrounds. Hence, the pursued design is possible in those points of the sampling grid that fall within the perturbation.

As well known [32], the L^2-norm of $\boldsymbol{\xi}$ will achieve its lowest values in these points. Then, the points to be selected to identify the virtual experiments (which we refer to as the *pivot* points) are simply chosen by observing the plot of the L^2-norm of $\boldsymbol{\xi}$ over the ROI and picking, among the S sampling points, the ones where this indicator function attains the smaller values. As usual in LSM, this plot also provides an estimate of the shape of the anomaly (but no information on its electromagnetic properties).

B. A new distorted-wave approximation

Once the design equation (8) has been solved and P pivot points have been selected, we build a set of P virtual

experiments. In each of these experiments, the total field is exactly given by:

$$\Psi_t^p(\underline{r}) = \sum_{\nu=1}^{N} \xi_\nu^p E_b^\nu(\underline{r}) + \mathcal{A}_i[\delta\tilde{\varepsilon}\Psi_t^p] = \\ = \Psi_b^p(\underline{r}) + \mathcal{A}_i[\delta\tilde{\varepsilon}\Psi_t^p], \qquad \underline{r} \in \Sigma \tag{9}$$

wherein $\boldsymbol{\xi}^p = \{\xi_1^p, ..., \xi_N^p\}$ is the regularized solution of (8) for the p-th pivot point (identifying the p-th virtual experiment).

The first addendum of the field's expression (9) is the background field arising in the reference scenario for the considered virtual experiment. This latter has the remarkable property of depending on the unknown permittivity perturbation $\delta\tilde{\varepsilon}$ in an implicit fashion through the combination coefficients $\boldsymbol{\xi}^p$.

Then, a first order approximation would be immediately achieved by neglecting the second term in (9). However, thanks to the features of the designed virtual experiments, a more refined field approximation can be considered. To this end one has to observe that the field scattered on Γ in the generic virtual experiment matches (in the L^2-norm) the Green's function for the reference background medium, g_b. Notably, such a scattered (anomalous) field does not depend on $\delta\tilde{\varepsilon}$, but only depends on the pivot point. As such it is known for any $\underline{r}$. Accordingly, the first order approximation (i.e., $\Psi_t \approx \Psi_b$) can be improved by assuming that the virtual anomalous field matches g_b not only on Γ, but everywhere. Hence, we can introduce the approximated total field

$$\Psi_t^p(\underline{r}) \cong \Psi_b^p(\underline{r}) + \Pi[g_b(\underline{r}, \underline{r}_p)], \qquad \underline{r} \in \Sigma \tag{10}$$

with $\underline{r}_p$ denoting the pivot point identifying the virtual experiment at hand and Π being a low-pass circular filter which avoids singularity of the approximated total field for $\underline{r} = \underline{r}_p$ [23].

The approximation introduced in (10) is equivalent to a prolongation of the anomalous field from Γ to the interior of Σ (and up to $\underline{r}_p$). Notably, it has the peculiar characteristic of depending on the specific perturbation at hand. In fact, coefficients $\boldsymbol{\xi}^p$ in the first term of (9) depend on the electromagnetic and geometrical properties of the scattering system at hand (see (8)).

As discussed in [23], [25] for the corresponding free space case, this approximation is superior to the straightforward linearization on which BA and DWBA are based, although of course has itself a limited validity due to the fact that near field effects and non-radiating components of the fields are neglected.

Approximation (10) relies on the applicability of the design equation (8), which is the case in all those situations wherein LSM is successful [23], [32], [35]. According to our experience and literature results, the LSM equation and its distorted formulation, are successful as long as the anomalies are comparable with the wavelength of the probing field. When the scattering system becomes too large (with respect to the probing wavelength) it is more difficult to induce a contrast source resembling the radiating properties of an elementary source point placed in the pivot point.

An accurate study of the validity range of the considered approximation has yet to be done. However, relying on the results in [25] it can be expected that approximation (10) starts to fail for increasing values of $\delta\tilde{\varepsilon}$ (with respect to $\tilde{\varepsilon}_1$). In particular, the larger $\delta\tilde{\varepsilon}$, the smaller electrical dimension (with respect to the probing wavelength) of the anomaly that can be retrieved.

By means of such an approximation, we finally come to a new linear distorted-wave data equation that reads:

$$\Psi_s^p(\underline{r}) = \mathcal{A}_e[\delta\tilde{\varepsilon}\Psi_t^p], \qquad \underline{r} \in \Gamma \tag{11}$$

with

$$\Psi_s^p(\underline{r}) = \sum_{\nu=1}^{N} \xi_\nu^p E_s^\nu(\underline{r}), \qquad \underline{r} \in \Gamma. \tag{12}$$

This equation provides the basis of the inversion technique detailed in the next section.

IV. Distorted-wave linear inversion via virtual experiments

In the following, we describe the implementation of the linear inversion method that takes advantage of the distorted-wave approximation introduced above.

The first step of the method requires to determine the virtual experiments, i.e., solve (8) and pick the pivot points. Let us assume that Σ has been sampled into an even grid of S points. Then, to counteract the ill-posedness of the problem, we exploit the singular value decomposition (SVD) of $\Delta\mathbf{E}_s$ and the Tikhonov regularization [32]. By doing so, the regularized solution reads:

$$\boldsymbol{\xi} = \sum_{i=1}^{T} \frac{\lambda_i}{\lambda_i^2 + \alpha^2} \langle \mathbf{g}_b, \boldsymbol{u}_i \rangle \boldsymbol{v}_i \tag{13}$$

wherein $\boldsymbol{v}_i$ and $\boldsymbol{u}_i$ are the right and left singular vectors of $\Delta\mathbf{E}_s$, respectively, λ_i denotes its i-th singular value, and $\langle \ , \ \rangle$ denotes the standard scalar product in L^2. Finally $T = min(N, M)$ and α is the Tikhonov regularization parameter chosen according to [34].

Then, we plot the indicator function:

$$\Upsilon(\underline{r}_s) = 20log_{10}\left[\sum_{n=1}^{N} |\xi_n|^2\right] \tag{14}$$

over the sampling grid, which both provides an estimate of the shape of $\delta\tilde{\varepsilon}$ and allows to pick the P pivot points. As discussed in [23], the choice of these latter is carried out evenly spacing the pivot points into the areas wherein Υ attains its lower values. Moreover, typically $P \simeq N$, where N is chosen according to guidelines given in [36] in order to collect non-redundant data.

The second step is the distorted-wave inversion, which is carried out by computing the approximated total field for each virtual experiments according to (10) and stacking the resulting P data equations into a single matrix equation as

$$[\mathbf{L}][\boldsymbol{\delta\tilde{\varepsilon}}] = [\boldsymbol{\Psi}_s] \ , \tag{15}$$

where $\mathbf{L}$ is the $(P \times M) \times N_c$ matrix whose entries are given by the Kronecker product between the $M \times N_c$ matrix encoding the reference scenario Green's function g_b as discretized for on

N_c pixels and the $P \times N_c$ matrix encoding the approximated (virtual) total field Ψ_t. Finally, $\boldsymbol{\delta\tilde{\varepsilon}}$ is the $N_c \times 1$ unknown vector and $\boldsymbol{\Psi}_s$ is the $(P \times M) \times 1$ vector containing the samples of the virtual anomalous field on Γ for the considered "multi-pivot / multi-static" arrangement.

A regularized solution of (15) can be achieved via the truncated SVD scheme (TSVD) that yields the following explicit solution:

$$\boldsymbol{\delta\tilde{\varepsilon}} = \sum_{j=1}^{N_T} \frac{1}{\sigma_j} \langle \boldsymbol{\Psi}_s, \boldsymbol{w}_j \rangle \boldsymbol{z}_j \tag{16}$$

wherein $\boldsymbol{z}_j$ and $\boldsymbol{w}_j$ are the right and left singular vectors of $\mathbf{L}$, respectively, and σ_j its singular values. The truncation index N_T can be conveniently set using the Picard' s plot, as suggested in [23].

It makes sense to compare the computational burden and the expected performances of the proposed method with respect to DWBA, as well as to EBA and DCSI.

With respect to DWBA, the additional computational burden comes from the first step of the procedure. In fact, the second step has exactly the same computational burden of DWBA. In both cases, one needs the knowledge of the Green's function of the reference scenario for all pairs of points $\underline{r}' \in \Sigma$, $\underline{r} \in \Gamma$, which has to be computed numerically (but for special cases). This task can be accomplished by first considering at each measurement position $\underline{r}_m$ an elementary source and solving the corresponding M forward scattering problems $\forall \underline{r} \in \Sigma$. Then, exploiting the reciprocity theorem, $g_b(\underline{r}, \underline{r}_m) = g_b(\underline{r}_m, \underline{r})$. In the first step, one also needs (see 10) the overall Green's functions for all the pivot points (i.e., all functions $g_b(\underline{r}_p, \underline{r}), p = 1, ..., P, \underline{r} \in \Sigma$). This latter can be numerically computed by solving P forward problems considering for each of them a unitary filamentary current placed in the considered pivot point, and computing the field for $\underline{r} \in \Sigma$. Moreover, the solution of the design equation requires a Singular Value Decomposition of a matrix whose dimension are $N \times M$. As these numbers are related to the number of experiments (and not to the number of pixels) such a step has a negligible computational weight even in case of 3D problems. As the solution of the additional forward problems which are needed to compute $g_b(\underline{r}_p, \underline{r})$ functions can be performed by taking advantage of parallel computing, the overall computational time can be kept only slightly larger than in DWBA. As we have already discussed, and going to show in Section V, this is however a price which is worth to be paid.

As far as comparison with EBA is concerned, note that such a method also consists in the sequence of two linear inversion steps. However, it requires the knowledge of the Green's function for all possible couples ($\underline{r} \in \Sigma$, $\underline{r}' \in \Sigma$) so that the computational burden is greatly increased with respect to DWBA and to the proposed method as well. Moreover, EBA is based on the assumption that interactions amongst distant points can be neglected. As such, it will be possibly accurate only in the presence of a sufficient amount of losses, which is obviously not the more general case. The DCSI, which can be considered an evolution of EBA, simultaneously looks for the contrast function and for an auxiliary function $\eta(\underline{r})$ representing a proportionality function amongst the incident field and the contrast source (for all views). As such, it is a fast method. However, one cannot be sure that such a function exists, as one can have a total field different from zero also in points where E_{inc} is zero, so that the auxiliary function cannot be used in these cases. Also note that such a proportionality assumption is deeply different in spirit from our approximation (10), where a part of the total field (the second term) is not proportional to E_{inc} at all. Hence, different performances and/or ranges of convenience are expected between DCSI and the proposed method. Moreover, it is worth noting that, to the best of our knowledge, both EBA and DCSI have been applied to the canonical homogeneous space case, and not to the distorted wave problem we are tackling in this paper.

V. Validation of the method

To give an assessment of the proposed approach, we have applied the above described procedure both to simulated data and experimental data taken from the 2005 Fresnel database [37] and we have compared the performance with those achieved with both DBWA and a modified version of EBA adapted to handle "distorted" problems.

The simulated data, the non homogeneous Green's function in eqs. (8), (15) as well as the approximation (10), have been computed by means of the COMSOL Multiphysics® package based on the finite element method. Also, for the Fresnel data, the reference total field at the receivers (not provided by the dataset), have been carried out by means of the COMSOL package. In simulated examples the number of transmitters and receivers has been set according to the guidelines in [36].

As final remark, let us discuss the computational burden of the method. By assuming the knowledge of the reference scenario, the evaluation of the Green's function and the background field required for (8),(10) and (11), are performed off-line and is not considered in the overall computational cost. As such, the proposed inversion method has a computational burden comparable with usual DWBA. As a matter of fact, our method requires to solve two linear problems and building the virtual fields. This latter has a negligible weight as it requires only linear combinations of the incident and the scattered field and a filtering operation based on the discrete fast Fourier transform. Whereas the solution of (8) consists of the computation of the SVD of a matrix of size $N \times M$ followed by the matrix multiplication needed to compute the indicator. Hence, this step also has a negligible computational burden. In the following numerical section, we give the time required by the method to cope with the overall imaging problem.

A. A proof-concept numerical example: imaging of two different anomalies embedded in the same scenario

As a first example, we have considered a lossless circular ROI ($\tilde{\varepsilon}_1 = 1.5$), with a diameter equal to $1.5\lambda_b$, embedded in a square imaging domain of side $2.5\lambda_b$ and discretized into 64×64 cells, at the working frequency of 1 GHz. The ROI is

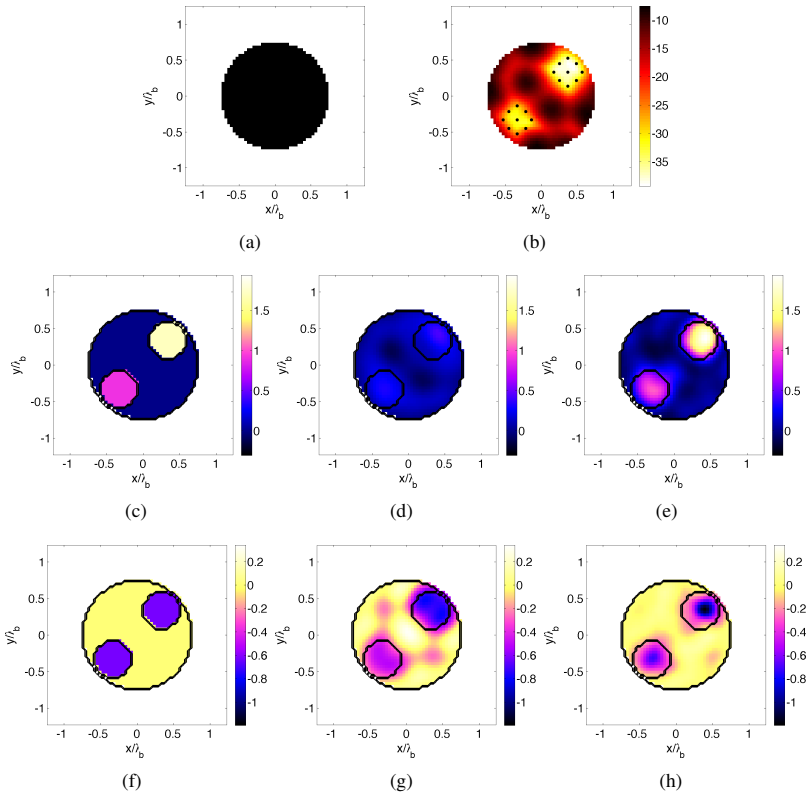

Fig. 1. Imaging of two cylindrical objects with different dielectric properties. (a) Geometry of the actual scenario, (b) logarithmic plot of the LSM map indicator (14) when normalized to its maximum with superimposed the pivot points ($P = 18$) marked as stars. Real part of the (c) actual unknown and the retrieved one by means of (d) the DWBA ($N_T = 109$) and (e) the proposed approach ($N_T = 120$). (f)-(h) Same as (c)-(e) but for the imaginary part. The black contour line represents the geometry of the actual scenario.

probed with $N = 24$ antennas placed on a circumference of radius $2.5\lambda_b$ and each probe acts both as transmitter and receiver to achieve a multiview-multistatic measurement configuration. The total field at $M = 24$ receivers has been measured when two cylindrical scatterers with different electromagnetic properties ($\varepsilon = 3.2$, $\sigma = 0.035$ S/m located at (0.3,0.3)λ_b and $\varepsilon = 2.4$, $\sigma = 0.035$ S/m located at (-0.3,-0.3)λ_b, respectively) and with a diameter of $\lambda_b/2$ have been considered inside the ROI, see Fig.1(a). To take into account the effect of the measurement noise, the useful signal defined as (5) has been corrupted by white random Gaussian noise with Signal-to-Noise Ratio SNR=15 dB. The accuracy of the result is appraised exploiting the mean square error,

$$err = \frac{||\delta\tilde{\varepsilon} - \hat{\delta\tilde{\varepsilon}}||^2}{||\delta\tilde{\varepsilon}||^2} \tag{17}$$

where $\delta\tilde{\varepsilon}$ is the actual perturbation profile, $\hat{\delta\tilde{\varepsilon}}$ the estimated one.

The first step of the procedure is the application of the LSM in order to identify the presence of the anomalies. Thereafter we take advantage of this energy indicator to choose the pivot points and to design the virtual experiments, see Fig.1(b). By solving the linearized problem (15) we obtain the result shown in Figs.1(e),1(h). As can be seen, the method is able to characterize the two different anomalies in a truly quantitative fashion, not only for the permittivity but also for the conductivity ($err = 25\%$) even though the reconstruction of this latter is slightly worse, outperforming the result achieves by means of DWBA ($err = 68\%$), see Figs.1(d),1(g). In particular, the regularization parameter in (16) has been set according to the Picard's plot as suggested in [23] for the VE driven approach and by discarding the singular values below the threshold of -15 dB (of the normalized singular values with respect to their maximum) for the DWBA inversion, since the Picard's plot can not be exploited due to the larger error model in the relevant scattering operator. The computational time of the example at hand is about 31 seconds. In particular, only 1 second is required for the first step and 30 seconds for the second step on a standard laptop PC, without exploiting parallel computing.

B. A proof of concept numerical example: imaging in radially stratified scenarios

In this section, the proposed approach has been tested against a complex scenario. It consists of a cross-section of a radially stratified structure made of three concentric layers and an inner core, see Fig.2(a). This structure can be thought as a rough phantom for different applications such as medical [38] and living tree trunk microwave diagnostics [39]. The dimensions and the dielectric properties of the layers are reported in Table I.

ε	$\sigma\ (mS/m)$	Thickness (cm)
6.2	2	1
22	5	4.8
16	1	8.67
9	0.5	10.6

TABLE I
GEOMETRICAL AND DIELECTRIC PROPERTIES (PERMITTIVITY AND CONDUCTIVITY) OF THE RADIALLY LAYERED SCATTERER FROM THE OUTERMOST TO THE INNERMOST LAYER

The diameter of the overall structure is 50 cm and it is embedded into an imaging domain of side 52.5 cm. The ROI is probed by means of a circular array of antennas placed at 12.5 cm from the outermost layer. The number of antennas is set to $N = 21$ at the working frequency of 650 MHz. The total field at the receivers is measured in presence of an elliptic shaped anomaly placed in the core at (4.2,-2) cm, representing a void ($\varepsilon = 1, \sigma = 0$) with axes' dimensions of 8 cm and 12 cm. In order to cope with an optimized imaging setup, a lossless matching medium with $\tilde{\varepsilon}_{host} = 4.7$ has been considered to guarantee a good coupling between the incoming incident wave and the structure.

In order to show the robustness of the proposed approach against the measurement noise, for this example we have corrupted the useful signal with two different levels of noise, i.e., SNR=20 dB and SNR=7 dB. The LSM energy indicators with superimposed the pivot points, considering a square sampling grid of 79×79 cells, are shown in Figs.2(b)-2(c) while the outcome of the inversion procedure is shown in Figs. 2(f),2(j) and Figs.2(g), 2(k). As can be seen, the proposed approach is able to achieve a quite satisfactory reconstruction of the unknown both for SNR=20 dB ($err = 38\%$) and SNR=7 dB ($err = 62\%$). In particular, as far as the real part of $\delta\tilde{\varepsilon}$, the procedure is able to recover the dielectric constant of the void, while, the approach is not able to retrieve the distribution of the imaginary part because of its very low value. In Figs.2(e),2(i) the retrieved electromagnetic properties by means of (distorted) EBA ($err = 147\%$) are shown. The adopted inversion procedure deals with the two linear step introduced in [17]. The first step is the inversion of the data equation in which the unknown is an auxiliary function. Thereafter, the Fredholm integral equation of second kind is solved by adopting a least square minimization. In this case, the result is not satisfactory, even if it outperforms the results obtained with the DWBA (not shown) in recovering the imaginary part, as can be noticed also from the cut of the actual and retrieved permittivity and conductivity profile reported in Figs.2(l)-2(o). Note that the physical feasibility conditions on the retrieved permittivity and conductivity profiles have been exploited in the visualization of the results in Figs.2(l)-2(o). In this case, the computational time is about 26 seconds, i.e., less than 1 second for the first step and about 25 seconds for the second one.

C. Experimental Data

In this section we test the proposed method against the experimental data of the 2005 Fresnel dataset [37]. This data set deals with non homogeneous scatterers obtained by considering several configurations of nested cylinders with different dimensions and materials. This experimental setup introduces the additional difficulty of dealing with a partially aspect limited configuration, in which however illuminations completely surround the targets. In particular, for each transmitter's position, the measurements are taken only on an arc of $240°$, excluding the $120°$ angular sector centered on the source. To apply the LSM to this kind of measurement configuration, a "zero filling" procedure has been exploited in arranging the matrix $\mathbf{\Delta E}_s$. This procedure consists in adding zero entries for those measurement locations not available in the experimental setup [33].

We have considered the two targets shown in Fig.3. The first one is the *FoamDielIntTM* target, in which a circular cylinder with radius 4 cm, with relative permittivity 1.45, embeds a smaller higher contrast circular cylinder of radius 1.5 cm and relative permittivity 3 ± 0.3, Fig.3(a). The second target is the *FoamTwinDielIntTM*, see Fig.3(b), which is made by placing an addition higher contrast circular cylinder in contact with the *FoamDielIntTM* target.

In both cases, to apply the proposed distorted wave method, we have assumed as reference scenario the foam cylinder, that implies to compute the background field for all the considered positions of the transmitters and receivers. Since this information is not supplied by the database, we have computed the reference field with the COMSOL 2D electromagnetic forward solver. It is worth noting that, in doing so, we have assumed as nominal position and nominal permittivity (of the foam cylinder) those provided by the dataset. However, since in the literature some inaccuracies in the position of the Fresnel scatterers have been experienced, it is worth noting that this could introduce a model error affecting the final result. Similar considerations can been argued for the background field, which has been performed considering an incident field obtained by means of a multipole expansion approach as suggested in [23].

The data for the *FoamDielIntTM* target have been directly supplied by the Institute Fresnel and consists of 72 incident fields and 61 measurements for each view. The ROI is a square region of side 20 cm hosting the foam cylinder and single frequency data have been processed at 3 GHz. It is worth noting we are assuming that a perturbation can be located either inside or outside of the foam cylinder. Fig.3(e) reports the qualitative image of the high contrast cylinder. Such an image has been achieved by adopting a 72×90 multiview-multistatic data matrix in which the data entries not available are replaced with zeros. As it can be seen, the solution of the distorted LSM equation allows to image the support of the anomaly so that a number of evenly spaced pivot points can be chosen within it. Fig.3(g) reports the final result obtained by applying the quantitative imaging step with respect to the selected pivot points. The retrieved permittivity, i.e., the retrieved perturbation $\delta\tilde{\varepsilon}$, is added to the nominal background scenario. Notably, the approach achieves

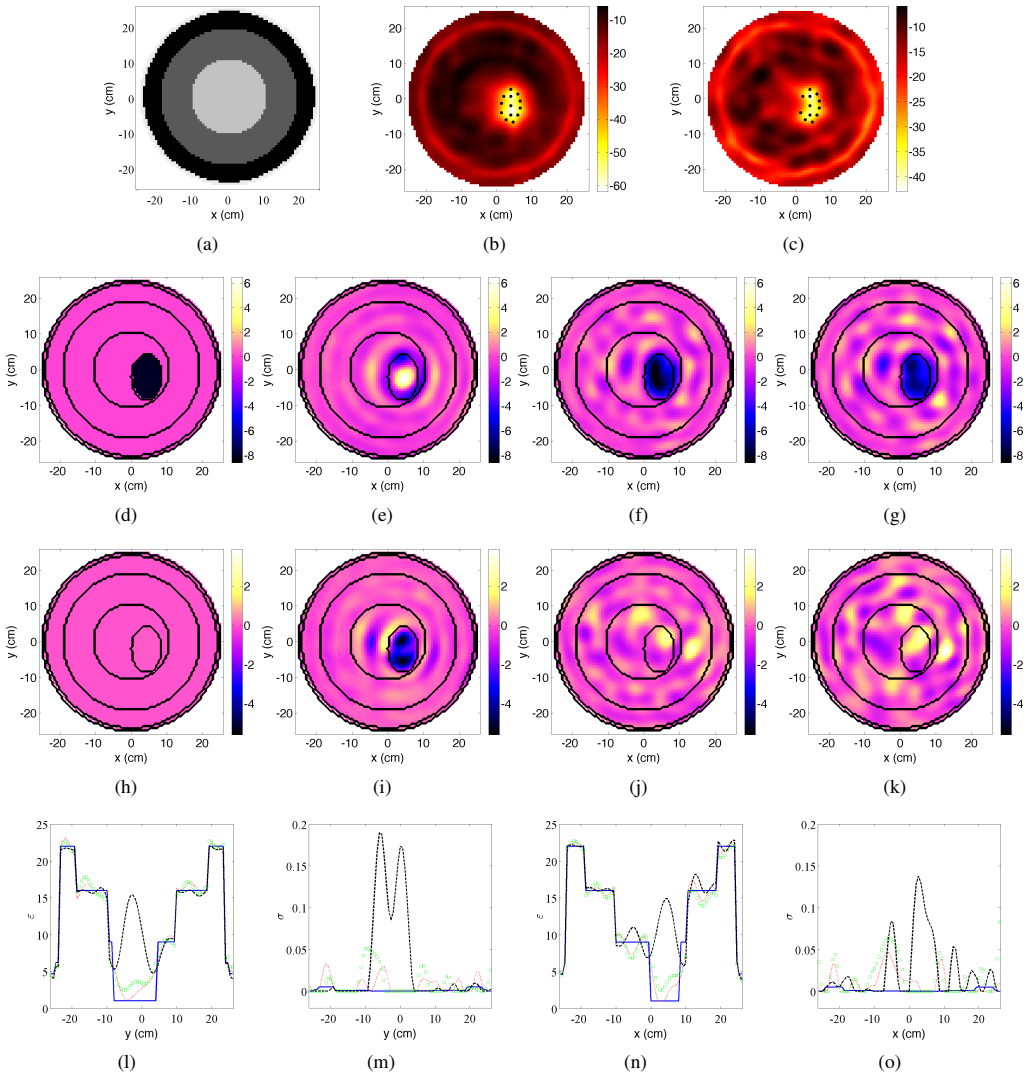

Fig. 2. Imaging of a target embedded in a radially stratified scenario. (a) Geometry of the nominal background. Logarithmic plot of the LSM map indicator (14) when normalized to its maximum with superimposed the pivot points marked as stars for (b) SNR=20 dB ($P = 13$) and (c) SNR=7 dB ($P = 12$) . Real part of the (d) actual unknown, the retrieved one by means of (e) the (distorted) EBA and by means of the proposed approach ($N_T = 100$) for (f) SNR=20 dB and (g) SNR=7 dB. (h)-(k) Same as (d)-(g) but for the imaginary part. The black contour line represents the geometry of the actual scenario. Cut at $x = 4.65$ cm of the (l) permittivity and (m) conductivity of the reference profile (solid blue line), retrieved profile by means of the proposed approach for SNR=20 dB (dotted red line), for SNR=7 dB (square-marked green line) and by means of the (distorted) EBA (dashed black line). (n)-(o) Same as (l)-(m) for a cut $y = -2$ cm.

a satisfactory reconstruction of the target especially when compared with the DWBA reconstruction (Fig.3(c)), see also Fig.3(i).

The outcome of the two steps for the *FoamTwinDielIntTM* target are shown in Fig.3(f) and 3(h), respectively. In this case, the dataset consists of $N = 18$ illuminations and $M = 241$ measurements for each view. Also in this case, the foam has been assumed as background scenario. The investigated domain is a square of side 17.5 cm, the working frequency is 4 GHz. The LSM indicator shown in Fig.3(f) has been obtained by adopting a 18×45 multiview-multistatic data matrix obtained by undersampling the original data and exploiting the "zero filling" procedure. On the basis of the retrieved support of the two cylinders, it is then possible to choose evenly spaced pivot points in order to apply the inversion strategy. Also in this case, the final result, shown in Fig.3(h), is very satisfactory from a quantitative point of view. As a matter of fact, see also Fig.3(j), the estimated permittivity values for both cylinders are in full agreement with the nominal ones, thus confirming the capability of the method to deal with the quantitative imaging task of non-weak target and then to outperform the standard DWBA, see Fig.3(d).

It is worth noting that physical feasibility conditions have been exploited in the visualization of the results by hard thresholding the obtained results. For these cases the overall

computational time takes about 1 minute.

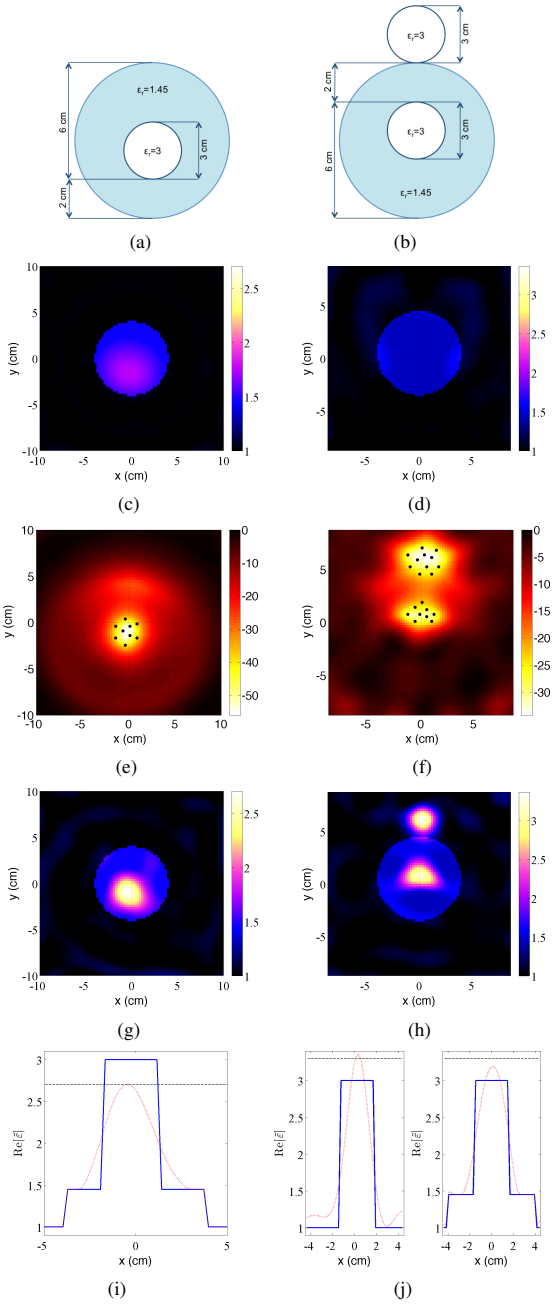

Fig. 3. Single frequency imaging results for the *FoamDielIntTM* (leftmost) and *FoamTwinDielIntTM* (rightmost) target. (c)-(d) Real part of the permittivity profile obtained by considering the retrieved permittivity superimposed to the reference one for DWBA. (e)-(f) Logarithmic LSM plot when normalized to its maximum with the selected pivot points ($P = 9$, $\tilde{P} = 20$), (g)-(h) same as (c)-(d) but for the proposed approach ($N_T = 84$, $N_T = 75$). (i) Cut of the permittivity profile at $y = -0.89$ cm, (j) at $y = 6.17$ cm and $y = 0.78$ cm: actual value (continuous blue line), retrieved profile (red dotted line) and accuracy level of the permittivity value provided by the Fresnel Institute (black dashed line).

VI. Conclusion

In this paper we have proposed a new method for the imaging of partially known scenarios. The new approach exploits jointly the emerging paradigm of the virtual experiments generalized to a distorted imaging problem, as well as a new approximation for the internal field. The main feature of the approach consists in taking into account the electromagnetic nature of the anomaly through a conversion of the original scattering experiments into new, software designed, virtual ones. As a matter of fact, by properly exploiting the virtual experiments paradigm, the problem can be suitably linearized with respect to the actual problem's unknown. As a result, the imaging problem can be tackled in an effective fashion within a linear framework and in a range of cases largely exceeding the popular distorted Born approximation, as well as other linearized approximations such as the Rytov or extend Born approximations. Notably, the proposed inversion method does not resort to iterative solution procedure and indeed its computational burden is the same as that of DBA based inversion, but for very negligible operations required to build the virtual experiments and the field approximation.

As remarkable result, the proposed method allows to successfully undertake the reconstruction of the inhomogeneous experimental Fresnel dataset. To the best of our knowledge, all previous results in the literature tackle the imaging problem related to these benchmark targets using non-linear and/or iterative methods, with obvious drawbacks and disadvantages.

On the other hand, it is interesting to note that this method, in a similar manner to the distorted Born iterated method (DBIM), lends itself to be easily exploited as the core of an iterated solution procedure which, being based on a wider range of validity with respect to the BA, should work finer than the DBIM, and can overcome the limits of the linearized method concerned with the homogeneous background.

Future work will be aimed at analyzing the class of scatterers for which the exploited approximation holds true. Of course, while a broader range of validity than DWBA can be foreseen, the approximation is expected to fail for large values of the permittivity and of the electrical dimensions of the unknown anomaly, with respect to the nominal background and the probing wavelength, respectively.

Finally, the method can be anyway implemented via regularized iterative solvers, especially for the solution of large scale problems concerned with the 3D case. As a result, some other kind of regularization approaches, like the multiplicative regularization and the compressive sensing, can be effectively exploited.

VII. Acknowledgement

The authors would like to thank the Dr. A. Litman and Dr. J.-M. Jeffrin from Institute Fresnel of Marseille, France, for providing the *FoamDielIntTM* dataset.

References

[1] M. Pastorino, *Microwave Imaging*. Wiley Online Library, 2010.
[2] D. Colton and R. Kress, *Inverse Acoustic and Electromagnetic Scattering Theory*. Berlin, Germany: Springer-Verlag, 1992.

[3] M. Bertero and P. Boccacci, *Introduction to Inverse Problems in Imaging*. Bristol, UK: Institute of Physics, 1998.

[4] T. Isernia, V. Pascazio, and R. Pierri, "A nonlinear estimation method in tomographic imaging," *IEEE Trans. Geosci. Remote Sens.*, vol. 35, no. 4, pp. 910–923, 1997.

[5] J. H. Rose and J. L. Opsal, "The inverse Born approximation: exact determination of shape of convex voids," *Review of progress in quantitative nondestructive evaluation*, vol. 2A, pp. 949–959, 1983.

[6] T. Grzegorczyk, P. M. Meaney, P. Kaufman, R. diFlorio Alexander, and K. D. Paulsen, "Fast 3-D tomographic microwave imaging for breast cancer detection," *IEEE Trans. Med. Imag.*, vol. 31, no. 8, pp. 1584–1592, 2012.

[7] M. Amin and K. Sarabandi, "Special issue on remote sensing of building interior," *IEEE Trans. Geosci. Remote Sens.*, vol. 47, no. 5, p. 12671268, 2009.

[8] A. J. Devaney and M. L. Oristaglio, "Inversion procedure for inverse scattering within the distorted-wave Born approximation," *Phys. Rev. Lett.*, vol. 51, pp. 237–240, Jul 1983.

[9] W. C. Chew and Y. M. Wang, "Reconstruction of two-dimensional permittivity distribution using the distorted Born iterative method," *IEEE Trans. Med. Imaging*, vol. 9, no. 2, pp. 218–225, 1990.

[10] C. Yu, M. Yuan, and Q. H. Liu, "Reconstruction of 3D objects from multi-frequency experimental data with a fast DBIM-BCGS method," *Inverse Probl.*, vol. 25, no. 2, p. 024007, 2009.

[11] C. Gilmore, P. Mojabi, and J. LoVetri, "Comparison of an enhanced distorted Born iterative method and the multiplicative-regularized contrast source inversion method," *IEEE Trans. Antennas Propag.*, vol. 57, no. 8, pp. 2341–2351, 2009.

[12] T. J. Cui, W. C. Chew, A. A. Aydiner, and S. Chen, "Inverse scattering of two-dimensional dielectric objects buried in a lossy earth using the distorted Born iterative method," *IEEE Trans. Geosci. Remote Sens.*, vol. 39, no. 2, pp. 339–346, 2001.

[13] A. G. Tijhuis, K. Belkebir, A. C. S. Litman, and B. P. de Hon, "Multiple-frequency distorted-wave Born approach to 2D inverse profiling," *Inverse Probl.*, vol. 17, no. 6, p. 1635, 2001.

[14] M. Slaney, A. C. Kak, and L. E. Larsen, "Limitations of imaging with first-order diffraction tomography," *IEEE Trans. Microwave Theory Techn.*, vol. 32, pp. 860 – 874, 1984.

[15] A. J. Devaney, "Inverse-scattering theory within the Rytov approximation," *Opt. Lett.*, vol. 6, no. 8, pp. 374–376, Aug 1981.

[16] T. M. Habashy, R. V. Groom, and B. R. Spies, "Beyond the Born and Rytov approximations: a non linear approach to electromagnetic scattering," *J. Geophys. Res.*, vol. 98, no. B2, pp. 1759–1775, 1993.

[17] T. M. Habashy and C. Torres-Verdn, "A two-step linear inversion of two-dimensional electrical conductivity," *IEEE Trans. Antennas Propag.*, vol. 43, pp. 405–415, 1995.

[18] A. Abubakar, T. M. Habashy, P. M. van den Berg, and D. Gisolf, "The diagonalized contrast source approach: an inversion method beyond the Born approximation," *Inv. Probl.*, vol. 21, pp. 685–702, 2005.

[19] W. P. Brown, "Validity of the Rytov approximation∗," *J. Opt. Soc. Am.*, vol. 57, no. 12, pp. 1539–1542, Dec 1967.

[20] M. Bevacqua, L. Crocco, L. D. Donato, and T. Isernia, "The virtual experiments: An emerging framework for the effective solution of inverse scattering problems," in *IEEE 9th European Conference on Antennas and Propagation (EuCAP)*, 2015.

[21] ——, "A "virtual experiments" framework for inverse scattering," in *IEEE 1st URSI Atlantic Radio Science Conference (URSI AT-RASC)*, 2015.

[22] M. Bevacqua, L. Crocco, L. D. Donato, T. Isernia, and R. Palmeri, "Exploiting virtual experiments for the solution of inverse scattering problem," in *IEEE International Conference on Electromagnetics in Advanced Applications (ICEAA)*, 2015, pp. 836 – 838.

[23] L. Crocco, I. Catapano, L. Di Donato, and T. Isernia, "The linear sampling method as a way for quantitative inverse scattering," *IEEE Trans. Antennas Propag.*, vol. 4, no. 60, pp. 1844–1853, 2012.

[24] L. Di Donato and L. Crocco, "Model based quantitative cross-borehole GPR imaging via virtual experiments," *IEEE Trans. Geosci. Remote Sens.*, vol. 53, no. 8, pp. 4178–4185, 2015.

[25] L. Di Donato, R. Palmeri, G. Sorbello, T. Isernia, and L. Crocco, "Assessing the capabilities of a new linear inversion method for quantitative microwave imaging," *Int. J. Antennas Propag.*, vol. 2015, 2015.

[26] M. Bevacqua, R. Palmeri, L. D. Donato, L. Crocco, and T. Isernia, "Microwave imaging via iterated virtual experiments," in *IEEE 10th European Conference on Antennas and Propagation (EuCAP)*, 2016.

[27] L. Di Donato, M. Bevacqua, L. Crocco, and T. Isernia, "Inverse scattering via virtual experiments and contrast source regularization," *IEEE Trans. Antennas Propag.*, vol. 63, no. 4, pp. 1669 – 1677, 2015.

[28] M. Bevacqua, L. Crocco, L. D. Donato, and T. Isernia, "An algebraic solution method for nonlinear inverse scattering," *IEEE Trans. Antennas Propag.*, Submitted.

[29] M. Bevacqua, L. Crocco, L. Di Donato, and T. Isernia, "Microwave imaging of non weak targets via compressive sensing and virtual experiments," *IEEE Antennas Wireless Propag. Lett.*, vol. 14, pp. 1035–1038, 2015.

[30] ——, "An algebraic solution method for nonlinear inverse scattering," *IEEE Trans. Antennas Propag.*, vol. 63, no. 2, pp. 601 – 610, 2015.

[31] L. Crocco, L. Di Donato, D. A. M. Iero, and T. Isernia, "An adaptive method to focusing in unknown scenario," *Prog. Electromagn. Res.*, vol. 130, pp. 563–579, 2012.

[32] F. Cakoni and D. Colton, *Qualitative methods in inverse scattering theory*. Berlin, Germany: Springer-Verlag, 2006.

[33] I. Catapano, L. Crocco, and T. Isernia, "On simple methods for shape reconstruction of unknown scatterers," *IEEE Trans. Antennas Propag.*, vol. 55, pp. 1431–1436, 2007.

[34] I. Catapano and L. Crocco, "An imaging method for concealed targets," *IEEE Trans. Geosci. Remote Sens.*, vol. 47, no. 5, pp. 1301–1309, 2009.

[35] L. Crocco, L. Di Donato, I. Catapano, and T. Isernia, "An improved simple method for imaging the shape of complex targets," *IEEE Trans. Antennas Propag.*, vol. 2, pp. 843–851, 2013.

[36] O. M. Bucci and T. Isernia, "Electromagnetic inverse scattering: retrievable information and measurement strategies," *Radio Sci.*, vol. 32, pp. 2123–2138, 1997.

[37] K. Belkebir and M. Saillard, "Testing inversion algorithms against experimental data: inhomogeneous targets," *Inverse Probl.*, vol. 21, no. 6, pp. S1–S3, 2005.

[38] S. Y. Semenov and D. R. Corfield, "Microwave tomography for brain imaging: Feasibility assessment for stroke detection," *Int. J. Antennas Propag.*, vol. 2008, 2008.

[39] L. Fu, S. S. Liu, and L. Liu, "Internal structure characterization of living tree trunk cross-section using GPR: Numerical examples and field data analysis," in *IEEE 15th International Conference on Ground Penetrating Radar (GPR)*, 2014, pp. 166–160.